Devising a Horizontal Chamber Array for Automotive OTA Tests in Random Line-Of-Sight

Andrés Alayón Glazunov[1], Per-Simon Kildal[1], and Madeleine Schilliger Kildal[1,2]
[1]Department of Signals and Systems, Chalmers University of Technology, Gothenburg, Sweden
[2]Bluetest AB, Gothenburg, Sweden

***Abstract*—In this paper we propose an approach to design a horizontal array antenna to reduce the uncertainty of reference measurements in Random Line-Of-Sight Over-The-Air testing in anechoic chambers. The main focus is on wireless communications testing to and from automotive vehicles. The proposed procedure allows to determine the size, the spacing and the number of elements of a horizontal array antenna resulting in an absolute error less than 1 dB. The analysis is based on presenting the output of the ideal digital threshold receiver model of the device under test as a Probability of Detection curve.**

***Index Terms*—vehicular, antenna, propagation, anechoic chamber, measurements, Random Line-Of-Sight.**

I. Introduction

Autonomous cars, i.e., self-driving cars with minimal human interaction, will soon become a reality in our roads. Many potential advantages with autonomous cars have been identified, such as, reduced traffic congestion, increased roadway capacity, improved environmental footprint, etc. However, autonomous cars require reliable and secure wireless connections to existing networks in order to achieve the desired improvements. Especially, in order to avoid accidents and to guarantee the safety of passengers and pedestrians, it will be crucial to set and meet performance requirements for communication with other cars on the road. Therefore, there is presently an acute need for Over-The-Air (OTA) testing of wireless communication to cars.

The OTA testing of wireless devices, e.g., handsets, can be performed in both anechoic chambers (with absorbing walls) and reverberation chambers (with reflecting walls) [1]. Reverberation chambers, if well designed, emulate the rich isotropic multipath (RIMP) environment. RIMP is a so-called edge environment emulating hundreds of waves impinging at the antenna and coming from uniformly distributed Angles-of-Arrival (AoA). RIMP is well-suited for both passive and active OTA testing [2]. Recently, a compact reverberation chamber and a compact anechoic chamber have been proposed for OTA testing of wireless connection to and between cars [3].

While the compact reverberation chamber for vehicular applications emulates the RIMP environment, the new compact anechoic chamber proposes to emulate the so called Random Line-of-Sight (RLOS) propagation channel. Indeed, autonomous cars travelling along highways will be often in a Line-of-Sight (LOS) connection to the base station. Likewise, communication to nearby cars will take place in LOS. However, the direction to the base station or neighboring car will change randomly depending on the relative orientations of the cars. Thus, the AoAs of the LOS relative to the car can be treated as random variables over the full (or in some cases limited) angular range in azimuth. The polarization of the impinging waves may, in a general RLOS environment, also be considered random due to the unpredictable positions and orientations of user devices relative the base station location [4]. On the other hand, for automotive tests the polarization in LOS may be considered known.

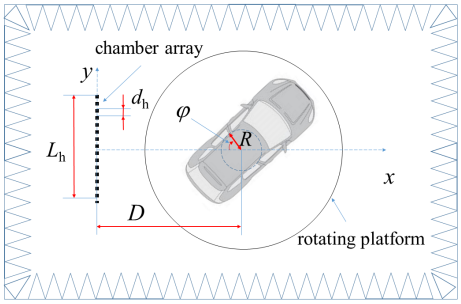

Fig. 1. Schematic representation of RLOS OTA measurement setup geometry in anechoic chamber.

The "typical" propagation channel is not known and might actually never be known. Therefore, a real-life hypothesis has been formulated: *if a wireless device is proven to work well in RIMP and RLOS, it will work well in all real-life environments* [4]. The communication characterization of devices in RIMP OTA is now rather well-understood for small to medium sized devices. However, work is still needed to fully extend the RIMP OTA to vehicular applications, but that is outside the scope of this paper. On the other hand, much less is known about the performance of a device operating in the RLOS propagation channel [5].

The main goal with this paper is to provide an initial study of the design of the RLOS OTA testing environment [5]. To our help, we have the ideal digital threshold receiver model. This model has significantly improved the OTA characterization of wireless devices, while keeping complexity down. The ideal digital threshold receiver model has been successfully employed to model the OTA throughput measured in reverberation chambers with excellent agreement with measurements for various MIMO-OFDM modes of operations [6]. The accuracy of RIMP OTA approaches an STD of 0.2 dB for efficiency- and power-related quantities [6], [7]. We aim at approaching this accuracy levels in RLOS OTA too.

II. RLOS OTA SETUP

The main goal with automotive RLOS OTA testing is to measure the communication performance of the DUT (Device Under Test) on car, e.g., throughput, on the horizontal or near-horizontal plane. Therefore, in the proposed RLOS OTA chamber there is no need to measure the complete radiation pattern; instead, measurements can be performed on the azimuthal plane. Moreover, the exact location of nulls in the radiation pattern of the tested antenna is not relevant due to the stochastic usage nature of the DUT. Hence, the requirements of RLOS chamber differ from traditional anechoic chambers, and thereby it can be realized at a much lower cost. Indeed, depending on the communication mode tested, the MIMO algorithms automatically take care of the polarization and the AoA impinging at the multi-port antenna. However, the testing system must ensure that the polarization, or if appropriate, two orthogonal polarizations of any kind are produced at the transmitting side. In LTE/LTE-A, MIMO algorithms are specified for single bitstream and for multiple bitstreams, i.e., the Maximum Ratio Combination (MRC) and the zero-forcing (ZF) are the most relevant, respectively [6], [11].

The proposed RLOS OTA method specifies a simplified measurement setup in a small anechoic chamber as shown in Fig.1. The car is located on a horizontal turntable of the same kind as in the RIMP OTA testing in a reverberation chamber as described in [3]. The rotation of the turntable provides the radiating near-field on a cylindrical surface around the vehicle. This is measured with a planar array antenna that we call chamber array antenna, or chamber array for short. The chamber array has a branched beamforming network. Therefore, the far-field is obtained directly at the output port of the chamber array [12]. This will therefore enable testing of active wireless communications in the far-field of the car, by connecting the output port directly to the wireless communication test instrument. The far-field can also be obtained at a small elevation angle by mechanically tilting the chamber array a few degrees to emulate the base station tilting. The chamber array must be dual-polarized or consist of several rows of parallel linearly polarized arrays to take advantage of MIMO in RLOS.

It is well-known that a uniform planar array can be considered as an array of linear arrays. As the first step, we therefore focus on the horizontal (azimuthal) behaviour of the fields in the testing zone defined by the location of the DUT on the tested car and relative the axis of the rotating platform see Fig.1. The chamber array consists of equidistantly spaced elements located at positions $\boldsymbol{r}_n = \left(n - \frac{N_{\rm ant}+1}{2}\right) d_{\rm h} \hat{\boldsymbol{y}}$ for $n = 1, 2, ..., N_{\rm ant}$, where $\hat{\boldsymbol{y}}$ is a unit vector defining the direction of the array axis, and $d_{\rm h}$ is the element spacing. We choose to define the total length $L_{\rm h}$ of the array by extending it to a $d_{\rm h}/2$ length outside the first and the last element, so that $L_{\rm h} = N_{\rm ant} d_{\rm h}$. The total field at a point $\boldsymbol{r}$ can be computed by superposition

$$\boldsymbol{E}(\boldsymbol{r}) = \sum_{n=1}^{N_{\rm ant}} \boldsymbol{G}(\hat{\boldsymbol{r}}_n) \frac{e^{-jk|\boldsymbol{r}-\boldsymbol{r}_n|}}{|\boldsymbol{r}-\boldsymbol{r}_n|} \ , \tag{1}$$

where $\boldsymbol{G}(\hat{\boldsymbol{r}}_n)$ is the far-field function of element n when referred to the phase reference point $\boldsymbol{r}_n$ of that element, and $\hat{\boldsymbol{r}}_n = (\boldsymbol{r} - \boldsymbol{r}_n) / |\boldsymbol{r} - \boldsymbol{r}_n|$. Let's consider a linearly polarized half-wavelength dipole oriented along the vertical z-axis and located at the testing zone. Thus, for this specific case, the normalized received power at point $\boldsymbol{r}$ can be computed as

$$\frac{P_{\rm rec}}{P_{\rm ref}} = \frac{|E_{\rm z}(\boldsymbol{r})|^2}{\frac{1}{\pi R^2}\int_0^R \int_0^{2\pi} |E_{\rm z}(\boldsymbol{r}(\rho,\varphi))|^2 \, \rho {\rm d}\rho {\rm d}\varphi} \ , \tag{2}$$

where $E_{\rm z} = \boldsymbol{E} \cdot \hat{\boldsymbol{z}}$, where $\hat{\boldsymbol{z}}$ is the unit vector along the z-axis. We assume that the distance from the center of the chamber array to the axis of the rotating platform is given by D(see Fig.1).

III. RECEIVER MODEL

The ideal digital threshold receiver model was introduced for throughput modelling in [5]. The model is based on the simple idea that in modern digital communication systems, the error rate goes very abruptly from only errors to free-of-errors in the Additive White Gaussian Noise (AWGN) channel. Then, in a fading environment, averaging over all the possible fading states gives the normalized average throughput [5]

$$\frac{\mathsf{TPUT}_{\rm av}(\gamma_{\rm av}/\gamma_{\rm th})}{\mathsf{TPUT}_{\max}} = \mathsf{PoD}(\gamma_{\rm av}/\gamma_{\rm th}) = 1 - \mathsf{CDF}(\gamma_{\rm th}/\gamma_{\rm av}) \ , \tag{3}$$

where PoD is the Probability of Detection (PoD) function, CDF is Cumulative Distribution Function (CDF) of the power at the output of the threshold receiver, $\gamma_{\rm av}$ is the available average received signal-to-noise ratio (SNR) under the AWGN assumption, $\gamma_{\rm th}$ is the threshold level of the receiver and may be obtained from conducted measurements. Hence, the relative throughput is then given by the PoD as shown in (3). Thus, throughput performance can be straightforwardly analyzed as shown in [8], [9].

IV. CHAMBER ARRAY DESIGN AND SIMULATION RESULTS

The testing zone in RLOS OTA is defined here by the circumference of radius R with center at the axis of the rotating platform (see Fig.1). The radius R is dictated by the outermost position of a DUT on car, e.g., on each of the lateral sides of the car. Hence, R would correspond to half the width of the car. In our study we aim at designing a chamber array that provides a target accuracy at $R = 1$ m. The target accuracy is based on the definition of two figures of merit. First, we consider the difference (in dB scale) between the measured power corresponding to $\mathsf{PoD} = 0.9$ at a fixed R. The corresponding normalized power (linear scale) is obtained as the average over for the testing zone here defined by the circle of radius R

$$\left(\frac{P_{\rm av}}{P_{\rm th}}\right)_{\rm dB} @0.9\mathsf{PoD} = 10\log_{10}\left(\mathsf{PoD}^{-1}(0.9)\right) \ , \tag{4}$$

where PoD^{-1} denotes the inverse function operation. The CDF is obtained from the measurements of (4) along the points in the circle of radius R (see Fig.1). It is worthwhile to note that $P_{\rm av}/P_{\rm th} = \gamma_{\rm av}/\gamma_{\rm th}$. Secondly, we consider the

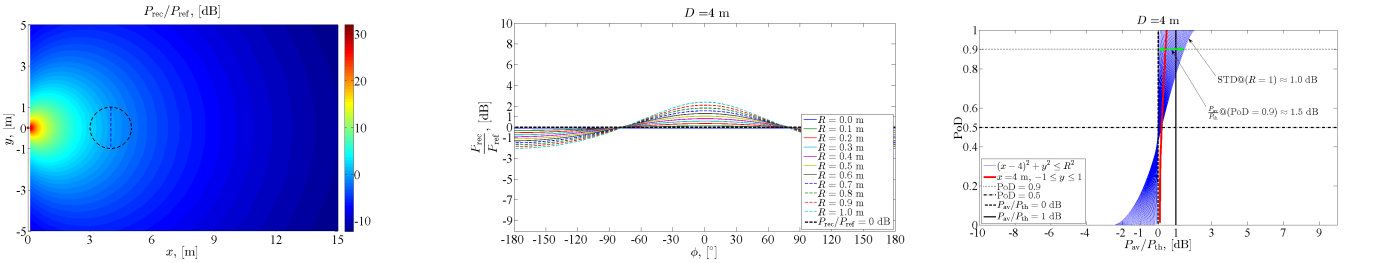

(a) (b) (c)

Fig. 2. Single Huygens source. (a) Normalized received power; the testing zone is given by the circle, (b) The normalized power v.s. the azimuth angle ϕ for points on a circle of radius R, (c) PoD corresponding to plots in (b). See Fig.1 for geometry.

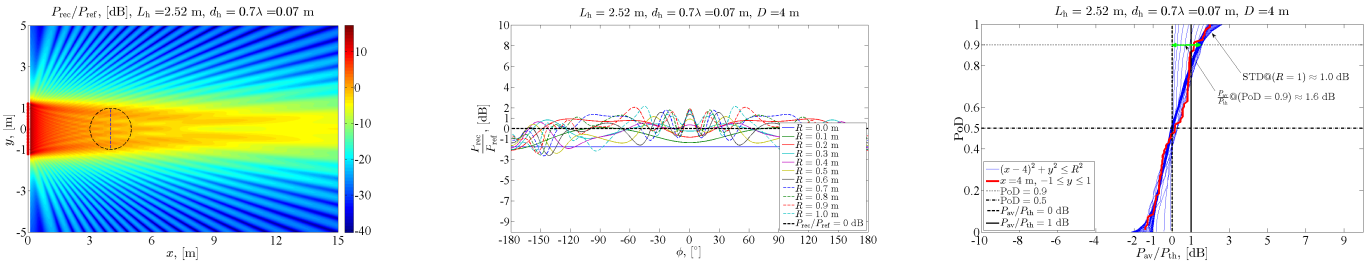

(a) (b) (c)

Fig. 3. Array antenna of length $L_{\rm h}=2.52$ m with 36 equidistant Huygens sources as elements. (a) Normalized received power; the testing zone is given by the circle, (b) The normalized power v.s. the azimuth angle ϕ for points on a circle of radius R, (c) PoD corresponding to plots in (b). See Fig.1.

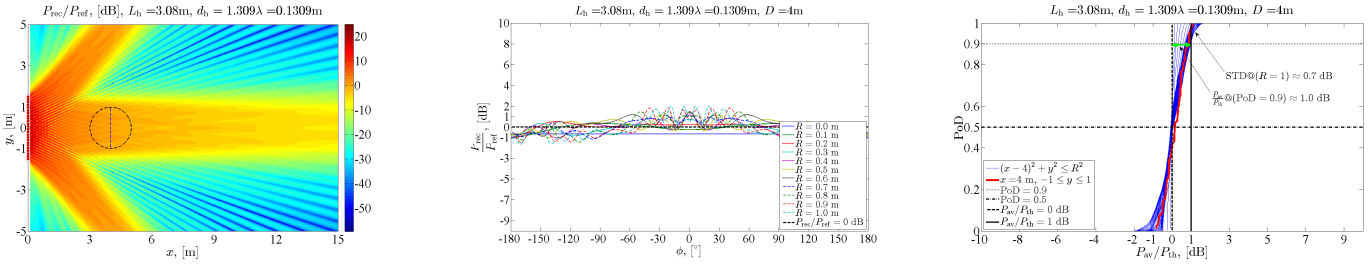

(a) (b) (c)

Fig. 4. Thinned and tapered array antenna of length $L_{\rm h}=3.08$ m with 24 equidistant Huygens sources as elements. (a) Normalized received power; the testing zone is given by the circle, (b) The normalized power v.s. the azimuth angle ϕ for points on a circle of radius R, (c) PoD corresponding to plots in (b). See Fig.1 for geometry.

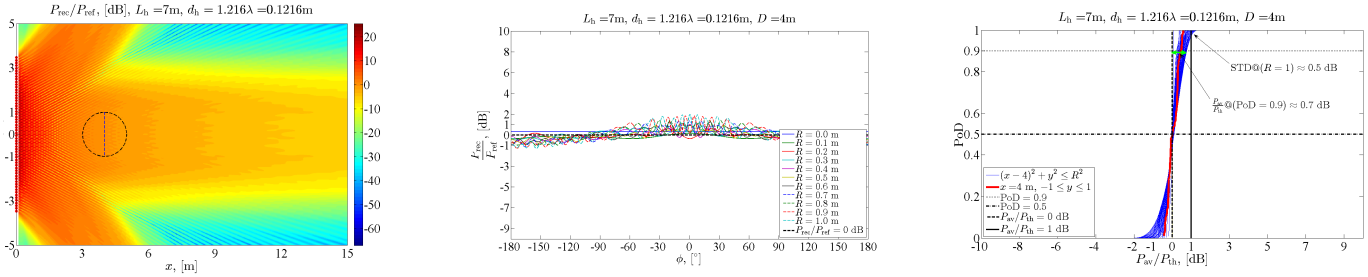

(a) (b) (c)

Fig. 5. Thinned and amplitude tapered array of length $L_{\rm h}=7.00$ m with 58 equidistant Huygens sources as elements. (a) Normalized received power; the testing zone is given by the circle, (b) The normalized power v.s. the azimuth angle ϕ for points on a circle of radius R, (c) PoD corresponding to plots in (b). See Fig.1 for geometry.

standard deviation STD of $P_{\rm av}/P_{\rm th}$ in dB scale. The accuracy of the reference measurements is good if the PoD-curve of the reference measurements taken over the area of the testing zone is as close as possible to the step function, i.e., fairly similar values obtained over the whole testing zone.

In order to simulate a compact RLOS OTA chamber we have chosen $D=4$ m. In the design of the horizontal chamber array we use the size of the array $L_{\rm h}$ and the element spacing $d_{\rm h}$ as design variables. Moreover, we consider vertically polarized Huygens sources as elements operating at the 3 GHz band. The computations are done according to the following five steps using MATLAB®. (**I**) In order to *avoid grating lobes* we set $d_{\rm h}=0.7\lambda$, where $\lambda=0.1$ m. We change R from 0 to 1 m in steps of $\lambda/8$, and $L_{\rm h}$ from 0.7λ to 7 m in steps of 0.7λ. (**II**) From the previous step we obtained that the "*target accuracy*" $(P_{\rm av}/P_{\rm th})_{\rm dB}\leq 1$ dB or STD ≤ 1 dB

is satisfied by certain combinations of $L_{\rm h}$ and R (Not shown here due to lack of space). It should be noted that if $R = 0$, then from (2) and (4) we see that the ratio will be exactly 0 dB. For all the other radii R, the target accuracy is achieved starting at a certain size size $L_{\rm h}$. We choose $L_{\rm h} = 3.08$ m at $d_{\rm h} = 0.7\lambda$ which gives an array with $N_{\rm ant} = 44$ elements as a starting point. (**III**) We then proceed with the *thinning* of the array, i.e., reducing the number of equidistant elements from $N_{\rm ant} = 44$ to $N_{\rm ant} = 1$, while keeping the total array length constant. (**IV**) From results in the previous step we obtained that the "target accuracy" is observed at all radii R if $N_{\rm ant} \geq 24$ (thinned array). Choosing this value with $L_{\rm h} = 3.08$ m, gives $d_{\rm h} = 1.309\lambda$ for the thinned array. (**V**) As a final step we apply a linear-in-dB *amplitude tapering* from 0 to -6 dB to 25% of the elements on each side of the array in order to reduce power variations across the testing zone.

Simulations results corresponding to various array sizes with or without thinning and tapering are shown in Fig.2 to Fig.5. The normalized received power on the x-y plane, the normalized received power along the circles of various radii from 0.1 m to 1 m, with steps of 0.1 m and the corresponding PoD curves are shown in each of the corresponding sub-figures a), b) and c), respectively. For the sake of comparison, results corresponding to a single vertically polarized Huygens source are shown in Fig.2. In this case, the coupling between the reference antenna and each element of the chamber array is determined by Friis equation. The variation of the receive signal in the testing zone increases with the radius R as shown in Fig.2b). The corresponding PoD curves are used to determine the deviation from the reference level according to (2). For a well-calibrated measurement it should be 0 dB. As can be seen from Fig.2c) the "error" at the $\mathsf{PoD} = 0.9$ is approximately 1.5 dB. Also, the normalized received power across the diameter going in parallel to chamber array (see Fig.2a) undergoes relatively small fluctuations as shown by the thicker PoD curve. In order to reduce this variations we can increase the size of the chamber array. In this case, a plane wave front is produced as a result of the superposition of spherical waves stemming from various equidistant sources. This is illustrated in Fig.3, where by choice of parameters there are no grating lobes. We see that while the "error" almost the same with a rather pronounced fluctuations (ripple) of the power in the testing zone (see Fig.3c)). This variation can be reduced by increasing the array size and by proper thinning and amplitude tapering as shown in Fig.4 with sub-figures. Clearly, grating lobes appear since $d_{\rm h} \geq \lambda$. However, better accuracy is achieved, while efficiently reducing the number of elements from 44 to 24. Additional accuracy improvement can be achieved at the expenses of a much larger array as shown in Fig.5 with sub-figures. This last point is clearly illustrated by the standard deviation (STD) computed over all data points obtained over the testing zone of radius $R = 1$ m. Estimated STD results are approximately 1.0, 1.0, 0.7 and 0.5 dB as indicated in each of the corresponding PoD plots.

V. Conclusion

A methodology has been proposed to generate a homogeneous reference power distribution over the testing zone in Random Line-Of-Sight Over-The-Air testing for automotive applications. Two figures of merit where used to define a target accuracy: the relative power at a certain probability of detection level, i.e., $\mathsf{PoD} = 0.9$, and the standard deviation of the relative power based on the probability of detection curve.

Tuning in the size, the spacing and the amplitude excitation tapering of the array elements proved essential to improve accuracy over the test zone. Future work will address the array behavior in the elevation angle to model base station tilting as well other ways to improve accuracy for an optimized chamber array.

This work has been supported by two projects from Swedens innovation agency VINNOVA, one within the VINN Excellence Center Chase at Chalmers and another via the program Innovative ICT 2013, and by internal support from Chalmers.

References

[1] A. A. Glazunov, V. M. Kolmonen, and T. Laitinen, "MIMO over-the-air testing," *in LTE-Advanced and Next Generation Wireless Networks: Channel Modelling and Propagation. Hoboken*, NJ, USA: Wiley, 2012, pp. 411–441.

[2] P.-S. Kildal and K. Rosengren, "Correlation and capacity of MIMO systems and mutual coupling, radiation efficiency and diversity gain of their antennas: Simulations and measurements in reverberation chamber," *IEEE Communications Magazine*, vol. 42, no. 12, pp. 102–112, Dec. 2004.

[3] P.-S. Kildal, A. A. Glazunov, J. Carlsson, A. Majidzadeh, "Cost-effective measurement setups for testing wireless communication to vehicles in reverberation chambers and anechoic chambers," Antenna Measurements & Applications (CAMA), 2014 IEEE Conference on , vol., no., pp.1,4, 16-19 Nov. 2014

[4] P.-S Kildal, "Rethinking the Wireless Channel for OTA testing and Network Optimization by Including User Statistic: RIMP, Pure-LOS, Throughput and Detection Probability," ISAP 2013.

[5] P.-S. Kildal, A. Hussain, X. Chen, C. Orlenius, A. Skårbratt, J. Asberg, T. Svensson and T. Eriksson, "Threshold Receiver Model for Throughput of Wireless Devices With MIMO and Frequency Diversity Measured in Reverberation Chamber," *IEEE AWPL*, vol.10, no., pp.1201,1204, 2011.

[6] A. Hussain, P.-S. Kildal, A. A. Glazunov, "Interpreting the Total Isotropic Sensitivity and Diversity Gain of LTE-Enabled Wireless Devices From Over-the-Air Throughput Measurements in Reverberation Chambers," *IEEE Access*, vol.3, no., pp.131–145, 2015.

[7] P.-S. Kildal, X. Chen, C. Orlenius, M. Franzén, C. Lötbäck Patané, "Characterization of Reverberation Chambers for OTA Measurements of Wireless Devices: Physical Formulations of Channel Matrix and New Uncertainty Formula," IEEE Transactions on Antennas and Propagation, Vol. 60, No. 8, pp. 3875-3891, Aug. 2012

[8] P.-S. Kildal and X. Chen, M. Gustafsson and Z. Shen, "MIMO Characterization on System Level of 5G Microbase Stations Subject to Randomness in LOS," *IEEE Access*, vol.2, no., pp.1062–1075, 2014.

[9] P.-S. Kildal, C. Orlenius, J. Carlsson, "OTA Testing in Multipath of Antennas and Wireless Devices With MIMO and OFDM," *Proceedings of the IEEE*, vol.100, no.7, pp.2145–2157, July 2012.

[10] H. Raza, A. Hussain, J. Yang, and P.-S. Kildal, "Wideband compact 4-port dual polarized self-grounded bowtie antenna," IEEE Trans. Antennas Propag., vol. 62, no. 9, pp. 4468–4473, Sep. 2014.

[11] P.-S. Kildal, X. Chen, M. Gustafsson, S. Zhengzhao, "MIMO Characterization on System Level of 5G Microbase Stations Subject to Randomness in LOS," Access, IEEE , vol.2, no., pp.1064–1077, 2014.

[12] P.-S. Kildal, Methods and apparatuses for testing wireless communications to vehicles, patent application number EP 14153281.2, 30 januari 2014.